ELECTROCHEMICAL DETERMINATION OF THE ANODE FILM RESISTANCE AND DOUBLE LAYER CAPACITANCE IN MAGNESIUM–MANGANESE DIOXIDE DRY CELLS

S. R. NARAYANAN and S. SATHYANARAYANA*

Department of Inorganic and Physical Chemistry, Indian Institute of Science, Bangalore 560 012 (India)

(Received June 15, 1984; in revised form January 15, 1985)

Summary

The transient and steady-state analysis of the galvanostatic discharge response of Mg–MnO_2 cells — in the absence of a dielectric breakdown of the passive film on Mg — yields valuable information on the resistance and capacitance of the protective film on the Mg anode. Theoretical analysis of the response curves has been completed, and a simple, reliable technique has been evolved to obtain, experimentally, the response data. Experimental data have been found to be in good agreement with theoretical analysis. The technique can be easily applied as a non-destructive tool for examining the stability of the film on Mg anodes and can be extended to anodes of other battery systems that involve reactive metals (*e.g.*, Li, Al, etc.) covered by a protective film. Several modes of failure of such cells may be predicted by applying the method proposed.

Introduction

Primary batteries based on reactive metal anodes such as magnesium and lithium are becoming increasingly important. Such batteries have a relatively high energy density and a long shelf life compared with conventional zinc–manganese dioxide (Leclanché) dry cells. In addition, the magnesium–manganese dioxide dry cell uses materials which are relatively cheap and plentiful.

The long shelf life of these batteries is mainly due to the presence of a protective, passive film on the anode surface that is produced during the fabrication of the cells. Inadequate passivation of the anode leads to prema-

*Author to whom correspondence should be addressed.

0378-7753/85/$3.30

ture failure of the cells during storage due to corrosion of the anode. On the other hand, excessive passivation of the anode entails a long delay time for the attainment of a steady-state cell voltage after initiation of discharge. An optimal passivation treatment for the anode is therefore one which produces a protective film with a minimal delay time during discharge.

The delay-time parameters of magnesium anodes are mainly governed by the resistance and dielectric strength of the passive film, as well as by the capacitance of the film-covered anode [1, 2]. It is of great practical importance to evolve techniques which will determine these properties of film-covered anodes in dry cells. For example, *in situ* measurement of film properties in assembled battery cells will assist greatly in the detection of weak electronic shorts in defective cells. Such internal electronic shorts will lead to a steep fall in the otherwise high impedance value of an undischarged cell.

The aim of the present investigation has been to develop a non-destructive electrochemical technique for the determination of the anode-film resistance and capacitance in magnesium–manganese dioxide dry cells. The method is based on the measurement and interpretation of voltage–time transients observed when the dry cells are discharged galvanostatically at current densities so small as to cause no change in the state-of-passivation of the anode. Criteria have been evolved to verify the non-destructive character of the method.

Background discussion

Principles of experiment

A galvanostatic pulse method has been proposed by Moshtev *et al.* [3] to determine the film resistance and capacitance of lithium anodes in Li–SO_2 and Li–$SOCl_2$ primary cells [4]. This work has several limitations, however. The film capacitance is calculated from the initial slope of a galvanostatic high-current, short discharge pulse, and the film resistance is obtained from the steady-state overvoltage observed during a galvanostatic smaller-current, longer discharge pulse. Such a sharp division of the cell response to pulse excitation is arbitrary since it amounts to a purely non-faradaic current flow at the anode during the short pulse (few μs) and, depending on both the nature of the anode metal and the state of passivation, the parameters and time-constants governing the faradaic and non-faradaic processes will be different. Further, pulse excitation involves a fairly high current density (1 - 100 mA cm^{-2} for D-size cells) which may lead to dielectric breakdown of the film, especially in short-pulse experiments.

In the light of these observations, it is desirable to carry out measurements at currents sufficiently small to eliminate any dielectric damage to the passive film on the anode, and to allow for the simultaneous flow of faradaic and non-faradaic currents in the interpretation of the entire transient. We could not find any report of such work in the literature.

Theoretical aspects

During the initial moments of discharge of an Mg–MnO_2 cell at normal rates (*i.e.*, $\sim 10^{-3}$ Q ampere or higher, where Q is the nominal ampere-hour capacity of the cell), the cell-voltage transient follows, typically, the course shown by curve 1 in Fig. 1. The main features of this curve are well understood [1, 2]. In brief, the cell voltage decreases appreciably across the passive-anode/solution interface due to the relatively high resistance to charge transfer presented by the film at the onset of discharge. The resulting high field causes metal ionisation as well as dielectric damage to the film. The accumulation of the anodic product creates dilatation stresses in the film, eventually leading to breakdown of the film at weak spots. The cell voltage then rises up to a value $V_{S,2}$ characteristic of the polarisation of the active anode at any given discharge current. On interrupting the discharge at time t_b, the open-circuit cell voltage initially rises to a high value due to the large negative potential of the film-free anode. Subsequently, a gradual, spontaneous passivation leads to a progressively more positive mixed potential at the anode and the cell voltage approaches the open-circuit value, V_o, that prevailed before discharge.

When the discharge rate is sufficiently small (typically 10^{-8} Q ampere or less), the cell-voltage transient follows a markedly different course as shown by curve 2 of Fig. 1. In particular, both the characteristic voltage dip on initiation of discharge (corresponding to anode-film breakdown) and the voltage overshoot on termination of discharge (corresponding to anode repassivation), seen in curve 1, are absent. Therefore, at low discharge rates, it follows that the discharge transient represents current flow through the cell without any anode-film breakdown. The flux of magnesium ions produced at the anode is apparently so small as to permit the attainment of a

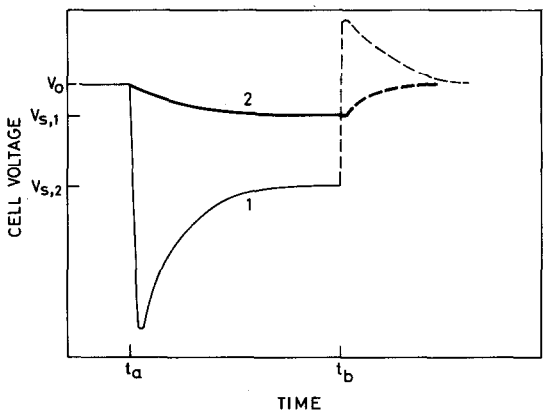

Fig. 1. Schematic of cell voltage *vs.* time during galvanostatic discharge and subsequent open-circuit recovery of Mg–MnO_2 dry cell. Discharge rates: 1, $\gtrsim 10^{-3}$ Q; 2, $\lesssim 10^{-8}$ Q; where Q is the current in amperes numerically equal to the nominal ampere-hour capacity of the cell; t_a is time of initiation of discharge; t_b is time of termination of discharge; V_o is the open-circuit cell voltage in the steady state; $V_{S,1}$ and $V_{S,2}$ are steady-state closed circuit voltages for 1 and 2, respectively. Dashed lines indicate open-circuit condition.

steady state without any damage to the film. Further, since the passive film on the anode has not suffered breakdown and the bare metal has not been exposed during the discharge transient, the open-circuit voltage transient after interruption of discharge at t_b does not exhibit any overshoot beyond V_o.

From these observations, the absence of a voltage undershoot below the steady-state, closed-circuit voltage on initiating a discharge, and the absence of any voltage overshoot above the open-circuit voltage on termination of discharge, may be taken as reasonable criteria to verify the stability of the passive anode-film during the test. Voltage–time transients of the type exhibited by curve 2 of Fig. 1 can therefore be used to evaluate, in a non-destructive way, the electrochemical characteristics of the film-covered anodes of primary cells.

Physical model

A theoretical interpretation of the voltage–time transient may be developed as follows.

Consider the galvanostatic discharge of an Mg–MnO_2 dry cell under conditions that allow the passive state of the anode to remain unaffected. The faradaic reaction at the anode is the ionisation of magnesium to form insoluble magnesium hydroxide* by hydrolysis. Therefore, elemental magnesium should be present at the site of the anodic reaction. Since diffusion of magnesium atoms through the passive film and subsequent ionisation at the film/solution interface is unlikely, the site of the reaction is the metal/film interface. An accumulation of the product of the anodic reaction at the interface (and, hence, a breakdown of the film by dilatation) does not occur when the total charge passed during the test is sufficiently small. In the present study, a current of 10^{-10} A cm^{-2} was passed for 5 min. The amount of charge passed (0.03 μC) corresponds to 0.015% of a monolayer of $Mg(OH)_2$ product (200 μC = 1 monolayer per cm^2). Thus, at discharge rates of the order of 10^{-8} Q ampere, or less, the anode film is unaffected.

Under the above conditions, the impedance of the cell is governed by the physically equivalent model shown in Fig. 2. The thin, dielectric, passive film of magnesium hydroxide is in contact with the metal on one side and the electrolyte on the other. Consequently, the film contributes a capacitance similar to that of a parallel-plate capacitor. Since the corrosion rate of magnesium is negligible, there is no contribution from faradaic pseudo-capacitance. Thus, the interfacial capacitance, C_1, arises entirely from the dielectric properties of the passive film. This capacitance is shown schematically as an accumulation of charge on either boundary of the film.

This physical model of the anode/solution interface implies that the interfacial capacitance is in parallel with the film resistance and the charge-

*The actual composition of the final anodic product may be complex, such as $MgO \cdot Mg(OH)_2 \cdot MgCrO_4$, etc. This aspect, however, is not essential for the understanding and interpretation of the transient.

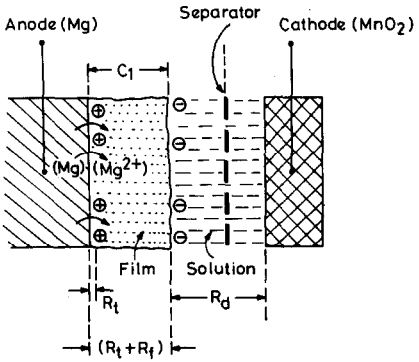

Fig. 2. Schematic of the physical elements contributing to the internal impedance in an Mg–MnO_2 dry cell before anodic breakdown. R_t is charge transfer resistance; R_f is film resistance; R_d is resistance of solution and separator; and C_1 is film capacitance.

transfer resistance. As a result, any instantaneous change in anode potential on application of a current step will be negligible, and the corresponding instantaneous change in cell voltage is governed by the resistance due to the solution and the separator, R_d. The impedance of the MnO_2 cathode is negligible by comparison, due to its large area and low polarisability.

In practical battery cells, R_d varies from a fraction of a milliohm to a few ohms, depending on the cell type. Thus, for the currents used in our tests, *i.e.*, $\sim 10^{-8}$ Q ampere, any instantaneous change in cell voltage will be a fraction of a microvolt or less and, hence, insignificant. Experimental data presented later have confirmed this conclusion for the Mg–MnO_2 dry cells under study.

It therefore follows that the determination of the internal resistance, or its components, of a battery cell with reactive metal anodes covered with a protective passive film is not ordinarily feasible by the potential-jump method in a non-destructive manner, *i.e.*, without breakdown of the film.

Equivalent circuit

In accordance with the above physical model, the electrical equivalent circuit of the cell sustaining a current, I, is shown in Fig. 3. Under the experimental conditions of the test (galvanostatic current: $\sim 10^{-8}$ Q ampere, or an anode current density: 10^{-10} A cm^{-2}; discharge time: 10 min; cell-voltage drop: 1 - 10 mV) the following assumptions can be made: (i) mass-transfer polarisation is negligible; (ii) R_t, R_d, R_f and C_1 are independent of potential and time. From the equivalent circuit in Fig. 3, with due regard to signs, *i.e.*, cathodic current is positive, single electrode potentials conform to the International convention,

$$V = E_c - E_a + IR_d \tag{1}$$

and

$$V_o = E_c - E_{a,cor} \tag{2}$$

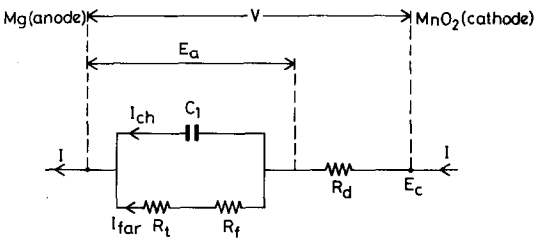

Fig. 3. Equivalent circuit of an Mg–MnO_2 dry cell sustaining a discharge current, I, before breakdown of the passive film on the anode. The branch currents are faradaic (I_{far}) and non-faradaic/charging current (I_{ch}) components during discharge. E_c is the cathode potential; E_a is the observable anode potential; and V is the cell-voltage. Other symbols are as in Fig. 2.

where $E_{a,cor}$ is the observed potential (in this case a corrosion potential) of the anode under open-circuit conditions. Further,

$$I = I_{far} + I_{ch} \tag{3}$$

and

$$I_{ch} = -C_1 \frac{dE_a}{dt} \tag{4}$$

In general, from electrode kinetics,

$$I_{far} = I_o\{\exp(-\alpha f\eta) - \exp(\beta f\eta)\} \tag{5}$$

where I_o is the exchange current; α and β are the apparent energy-transfer coefficients for the cathodic and anodic partial reactions; $f = nF/RT$; and η is the true overpotential, $(E - E_{rev})$, for the charge transfer reaction at the given electrode.

Description of the discharge transient

For reactive metal anodes covered with a protective passive film, as in the present case, the open-circuit potential is not a reversible potential but a mixed potential, namely, the corrosion potential. Thus, the exchange current is to be replaced by I_{cor}. The true overpotential, η, is the observed overpotential corrected for any potential drop across the passive film. This potential drop is given by $I_{far}R_f$.

Hence, with due regard to signs, the true overpotential is given by:

$$\eta = E_a - E_{a,cor} + I_{far}R_f \tag{6}$$

Consequently, the faradaic component is now given by:

$$I_{far} = I_{cor}[\exp\{-\alpha f(E_a - E_{a,cor} + I_{far}R_f)\} - \exp\{\beta f(E_a - E_{a,cor} + I_{far}R_f)\}] \tag{7}$$

Equations (1) - (7) may be combined suitably to eliminate $(E_a - E_{a,cor})$, I_{far} and I_{ch}, as shown below:

From eqns. (1) and (2):

$$\delta V = (V_o - V) = (E_a - E_{a,cor}) - IR_d \tag{8}$$

From eqns. (4) and (8):

$$I_{ch} = -C_1 \frac{d(\delta V)}{dt} \tag{9}$$

From eqns. (3), (8) and (9):

$$\begin{aligned} E_a - E_{a,cor} + I_{far}R_f &= (\delta V + IR_d + I_{far}R_f) \\ &= \{\delta V + IR_d + (I - I_{ch})R_f\} \\ &= \delta V + IR_d + \left\{I + C_1 \frac{d(\delta V)}{dt}\right\} R_f \\ &= \delta V + R_f C_1 \frac{d(\delta V)}{dt} + I(R_d + R_f) \end{aligned} \tag{10}$$

Finally, substituting eqn. (10) into eqn. (7), and putting $R_\Omega = R_d + R_f$, yields:

$$\begin{aligned} I = -C_1 \frac{d(\delta V)}{dt} + I_{cor}\Bigg[&\exp\left\{-\alpha f\left(IR_\Omega + \delta V + R_f C_1 \frac{d(\delta V)}{dt}\right)\right\} \\ &- \exp\left\{\beta f\left(IR_\Omega + \delta V + R_f C_1 \frac{d(\delta V)}{dt}\right)\right\}\Bigg] \end{aligned} \tag{11}$$

The solution of eqn. (11) is simple when it is recognised that the maximum value of δV in the experiment is limited to ~10 mV. The value of IR_Ω is negative at the anode during test discharge while its numerical value cannot exceed δV. Therefore, the term $(IR_\Omega + \delta V)$ is substantially smaller than 10 mV.

Further, the term $R_f C_1(d(\delta V)/dt)$ is always negative at the anode under discharge. The numerical value of this term may be large at the initial moments of discharge, but in the later stages of the transient the magnitude will be small since $d(\delta V)/dt \to 0$ as a steady state is approached. Hence, except at the initial moments of the transient, it is reasonable to assume that:

$$IR_\Omega + \delta V + R_f C_1 \frac{d(\delta V)}{dt} \ll \frac{1}{\alpha f} \quad \text{or} \quad \frac{1}{\beta f} \tag{12}$$

The validity of this assumption with regard to the third term on the left-hand side of the inequality can also be verified as follows. The maximum value of $R_f C_1$ can be estimated as the time taken for δV to reach about 66% of the final value, and $d(\delta V)/dt$ is obtainable from the experimental data. The exponential terms in eqn. (11) can then be linearised to give a simplified differential equation for the transient, *viz.*,

$$I = -C_1 \frac{d(\delta V)}{dt} - (\alpha + \beta) f I_{cor} \left(I R_\Omega + \delta V + R_f C_1 \frac{d(\delta V)}{dt} \right) \quad (13)$$

Solution of eqn. (13) gives:

$$\delta V = -(R_t + R_\Omega) I + K[\exp - \{t/(R_t + R_f)C_1\}] \quad (14)$$

where $R_t = 1/(\alpha + \beta) f I_{cor}$ and K is the integration constant. The latter constant cannot be evaluated at this stage since the initial conditions ($t = 0$) are excluded in the derivation of eqn. (14).

Comparison of theory with experiment

A comparison of experimental data with eqn. (14), that describes the transient, can be carried out as follows.

From eqn. (14):

$$\ln \left\{ - \frac{d(\delta V)}{dt} \right\} = \left[\ln \left\{ \frac{K}{(R_t + R_f)C_1} \right\} \right] - \frac{t}{(R_t + R_f)C_1} \quad (15)$$

Hence, a plot of ln $\{-(d(\delta V)/dt)\}$ *vs.* t should give a straight line. The slope of this line yields the value of $(R_t + R_f)C_1$.

The steady state value of δV, namely, Lim (δV), is obtained from eqn. (14), *i.e.*, $t \to \infty$

$$(\delta V)_\infty = -(R_t + R_\Omega) I$$
$$= -(R_t + R_f + R_d) I \quad (16)$$

The negative sign arises on the right hand side of eqn. (16) because the current, I, through the test electrode (anode) itself has a negative sign, and therefore the term δV is positive. The slope of $(\delta V)_\infty$ *vs.* I (the experiments being with different values of the test current in the specified range) yields the quantity $(R_t + R_f + R_d)$.

The internal resistance of the cell measured by conventional steady-state techniques, with test currents $\sim 10^{-3}$ Q ampere, is independent of R_f since the passive film on the metal anode would have necessarily broken down in such a discharge. The internal resistance thus obtained (or taken from manufacturers' data sheets) yields $(R_t + R_d)$ which is almost entirely R_d in practical cells due to the dominant role of the resistance of solution and separator.

By combination of the results so obtained, the values of the desired parameters R_f and C_1 may be readily calculated.

Open-circuit recovery transient

The differential equation for the open-circuit voltage recovery transient can be written down from eqn. (11) by setting $I = 0$. Thus:

$$C_1 \frac{d(\delta V')}{dt} = I_{cor} \left[\exp \left\{ -\alpha f \left(\delta V' + R_f C_1 \frac{d(\delta V')}{dt} \right) \right\} - \right.$$

$$-\exp\left\{\beta f\left(\delta V' + R_f C_1 \frac{d(\delta V')}{dt}\right)\right\}\Bigg] \quad (17)$$

The prime sign (′) has been used to indicate the open-circuit condition.

Towards the final stages of the transient $d(\delta V')/dt \rightarrow 0$ and, hence, the following condition holds:

$$\left[\delta V' + R_f C_1 \frac{d(\delta V')}{dt}\right] \ll \frac{1}{\alpha f} \text{ or } \frac{1}{\beta f}$$

The term $\delta V'$ is less than 10 mV due to the experimental situation adopted prior to current interruption. However, unlike in the case of the discharge transient, $d(\delta V')/dt$ has the same sign (*i.e.*, positive) as $\delta V'$. Hence, the inequality indicated should be verified with experimental data. When this condition is valid, eqn. (17) simplifies to:

$$C_1 \frac{d(\delta V')}{dt} = -(\alpha + \beta) f I_{cor}\left\{\delta V' + R_f C_1 \frac{d(\delta V')}{dt}\right\} \quad (18)$$

The solution of eqn. (18) is readily found to be:

$$\delta V' = K'[\exp - \{t/(R_t + R_f)C_1\}] \quad (19)$$

where K' is the integration constant.

A comparison of eqn. (19) with eqn. (14) shows that no new information is derived from the analysis of the open-circuit transient. In fact, between the discharge transient and the open-circuit transient, the former should be preferred as it is more accurate with respect to the fulfilment of the linearisation condition.

"Initial-slope method" for determination of capacitance

It is also of interest to analyse theoretically the situation which prevails during the initial moments of the discharge transient, *i.e.*, when $d(\delta V)/dt$ is numerically large compared with its value at the later stages.

$$I_{far} = I_{cor}[\exp\{-\alpha f(\delta V + IR_d + I_{far}R_f)\} - \exp\{\beta f(\delta V + IR_d + I_{far}R_f)\}] \quad (20)$$

From eqns. (3), (8) and (20):

$$I = -C_1 \frac{d(\delta V)}{dt} + I_{cor}[\exp\{-\alpha f(\delta V + IR_d + I_{far}R_f)\} - \exp\{\beta f(\delta V + IR_d + I_{far}R_f)\}] \quad (21)$$

Therefore,

$$\lim_{t \rightarrow 0}\left[-\frac{1}{I}\frac{d(\delta V)}{dt}\right] = \frac{1}{C_1}\left[1 - \frac{I_{cor}}{I}\{\exp[-\alpha f(\delta V + IR_d + I_{far}R_f)] - \exp[\beta f(\delta V + IR_d + I_{far}R_f)]\}\right] \quad (22)$$

Equation (22) points to the significant conclusion that the conventional method of using the initial stages of the voltage–time transient to calculate C_1, *i.e.*,

$$\lim_{t \to 0} \left[-\frac{1}{I} \frac{\mathrm{d}(\delta V)}{\mathrm{d}t} \right] = \frac{1}{C_1},$$

is in error to the extent of the second term inside the parentheses in eqn. (22). It is only when $I_{cor} = 0$ (or, in the case of a redox reaction, the exchange current is zero) that there is no error for the measurement of C_1 with a cell. Otherwise, there is an error in the determination of C_1 for any value of R_f, since IR_d is never zero for a cell. For single electrode studies with a properly positioned Luggin tip and reference electrode, however, where δV is to be replaced with η, $IR_d = 0$; also $\eta \to 0$ as $t \to 0$. Hence, if R_f is also zero,

$$\lim_{t \to 0} \left\{ -\frac{1}{I} \frac{\mathrm{d}\eta}{\mathrm{d}t} \right\} = \frac{1}{C_1}$$

In summary, for a two-terminal cell, the film resistance, R_f, and the film capacitance, C_1, can be evaluated in a non-destructive manner through the steps outlined above.

Experimental

Cells

Tests were conducted on commercial CL-size magnesium–manganese dioxide primary dry cells that were supplied by Messrs. Bharat Electronics Ltd., Pune. Both freshly manufactured cells, as well as cells stored at ambient temperature for over three years, were examined. The magnesium anode in these cells had a passivation coating of chromate and other inhibitors. The nominal capacity of these cells was 2.5 A h when discharged at a $Q/6$ rate to a cut-off voltage of 1.3 V at 28 °C.

Electrical circuit

An electrical circuit (shown in Fig. 4) was developed to carry out the studies on the cell-discharge transient under galvanostatic conditions. The circuit has the following important features:

(i) Since the range of currents to be used in the experiments has been identified as 10^{-8} - 10^{-9} A cm^{-2}, the cell voltage has to be monitored by an electrometric amplifier whose sensing currents are much smaller than the test currents. The electrometric amplifier is interfaced with a recorder to obtain the V–t plot.

(ii) Under the above conditions, the fall in cell voltage is of the order of a few mV only. Therefore, a voltage back-off employing a nickel–cadmi-

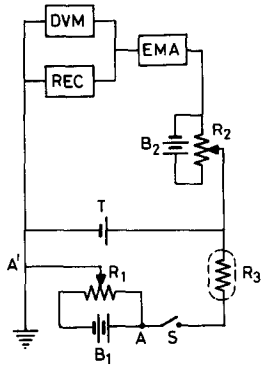

Fig. 4. Experimental set-up for discharge studies on Mg–MnO_2 dry cells at extremely low discharge rates. T is the test cell; R_1 is a 10 kΩ, ten-turn, helical potentiometer; R_2 is a 10 kΩ, single-turn potentiometer; R_3 is a 10 MΩ, high-stability, current-limiting resistor; B_1 and B_2 are nickel–cadmium cells at 50% state-of-charge; DVM is a digital voltmeter; REC is a recorder with 0.4 mV/cm sensitivity; EMA is an electrometric amplifier with input impedance $> 10^{12}$ Ω and unit gain.

um cell, B_2, and a variable resistance, R_2, is necessary to record the transient at the highest possible sensitivity of the recorder.

(iii) The series current-limiting resistor, R_3, has a precisely known value in the region of 10 MΩ. The value of R_3 is determined by preliminary trials with cells so that R_3 is about a hundred times more than the internal resistance of the cell with the anode film intact. With such a value of R_3, the cell current is practically constant throughout the experiment, notwithstanding the drop of 1 - 10 mV in cell voltage during this time. Further, R_3 has to be shielded to prevent noise pick-up which could otherwise reach as much as 10% of the signal level ($V_o - V_s$). The circuit is carefully designed to avoid ground loops and such other spurious faults.

(iv) The potentiometer R_1 is adjusted such that the difference in voltage between the test cell, T, and that tapped across R_1 acts as a driving force for discharge. By varying the tapped voltage across R_1, the experiment can be carried out at different values of the discharge current. This avoids the need to change R_3 from one experiment to another.

(v) Nickel–cadmium cells, B_1 and B_2, are used at 50% state-of-charge so that the voltage change of these (about 1 μV/μA h) is negligible during the experiment. This ensures a proper galvanostatic regime for the test-cell discharge at nano-ampere levels and a recording of the voltage changes at the μV level.

The sequence of operations during a typical experiment is as follows. The open-circuit voltage of the cell is noted. The voltage difference between points A and A′ is now adjusted with R_1 to arrive at the desired current through the cell when the switch S is closed, *e.g.*, with 200 mV and 10 MΩ (R_3) in series, a current of 2×10^{-8} A can be driven. By necessity, an electrometer has to be used in all voltage measurements involving the test cell. The open-circuit voltage is backed off by adjusting R_2 so as to effect a full-

scale recording of the expected voltage change (1 - 10 mV) on the recorder. The switch S is then closed to commence discharge and the V–t curve recorded. The actual current through the cell is calculated from the voltage drop across R_3. When the rate of change of voltage with time is about 1% of the initial rate of change, a steady state is assumed to have been reached. The switch is now opened and the open-circuit voltage recovery recorded. The experiment is repeated with the same cell for five values of current in the range identified where disruption of the anode film does not occur.

Calculation of voltage derivatives

The derivatives required (see eqn. (15)) were obtained by graphical differentiation of the experimental voltage–time transient. The recorder tracing of the transient was interpolated to get individual data points which were plotted on a large-scale graph to draw a smooth curve of best-fit. A plane metal mirror was aligned at the chosen point on the curve to locate the normal to the tangent at that point. By reading off the coordinates at the intersection of the axes by the mirror edges, the derivatives could be calculated with an accuracy of about 1%.

The steady-state data from a set of five cells were used to calculate the total internal resistance $(R_t + R_f + R_d)$ according to eqn. (16). The complete analysis of the transient data according to eqns. (15) and (19) was carried out for two of the cells at each discharge current employed. A separate set of cells was used to obtain $(R_t + R_d)$, *i.e.*, the internal resistance of the cell under usual, relatively high-rate, discharge.

Results and discussion

Cell discharge and recovery transients

Typical cell voltage *vs.* time plots recorded under different conditions are given in Figs. 5 - 7.

It can be seen from Fig. 5 that the initial voltage minimum before the attainment of the steady state on-load voltage and the subsequent open-

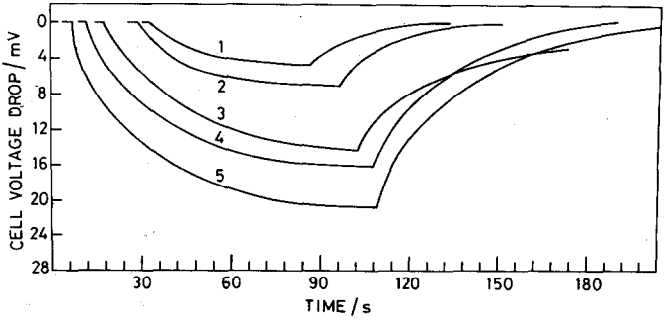

Fig. 5. Galvanostatic discharge and subsequent open-circuit recovery transients for an Mg–MnO_2 dry cell (nominal capacity 2.5 A h) at 1, 0.010; 2, 0.015; 3, 0.020; 4, 0.025; 5, 0.030 μA.

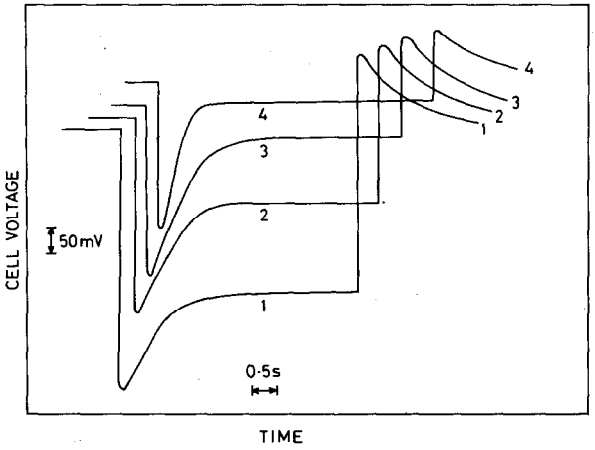

Fig. 6. Galvanostatic discharge and subsequent open-circuit transients for an Mg–MnO_2 dry cell (nominal capacity 2.5 A h) at 1, 500; 2, 200; 3, 100; 4, 50 mA.

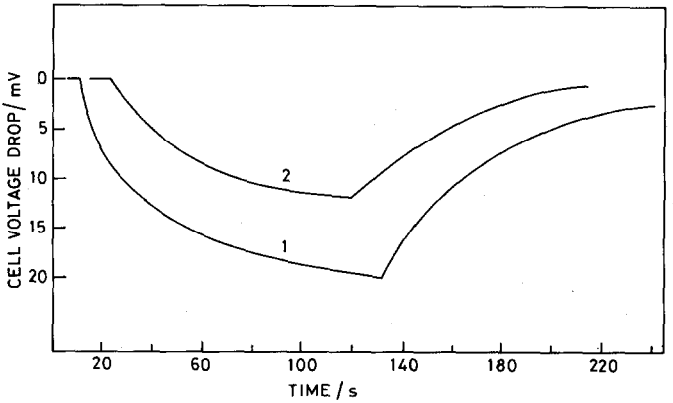

Fig. 7. Galvanostatic discharge and subsequent open-circuit recovery transient of an Mg–MnO_2 dry cell (nominal capacity 2.5 A h): 1, stored for 3 years at ambient temperature prior to test; 2, same cell after injecting 1 ml of water and equilibrating for 24 h before the test. Discharge current in both cases 0.01 μA.

circuit voltage overshoot above the final open-circuit voltage, which are characteristic of anode film breakdown processes, is absent when the discharge current is of the order of 10^{-8} Q ampere or less (compare with Fig. 6).

Cells stored for a long time and therefore subjected to capacity loss by a cell dry-out mechanism are seen to recuperate on being injected with water. This is demonstrated in Fig. 7. The internal resistance for a stored cell falls to a lower value when treated with a small quantity of water. This phenomenon, *viz.*, the film resistance of cells under storage being substantially higher than the corresponding value for fresh cells, can be used to monitor, non- destructively, the shelf-life of stored cells, since the loss of moisture is a dominant cause of poor shelf-life in Mg–MnO_2 cells.

Film resistance

Typical plots of $(\delta V)_\infty$ *vs.* I obtained for a cell under different discharge rates are shown in Figs. 8 and 9. The value of the total internal resistance of the cell (R_i) as a function of the discharge current is plotted in Fig. 10.

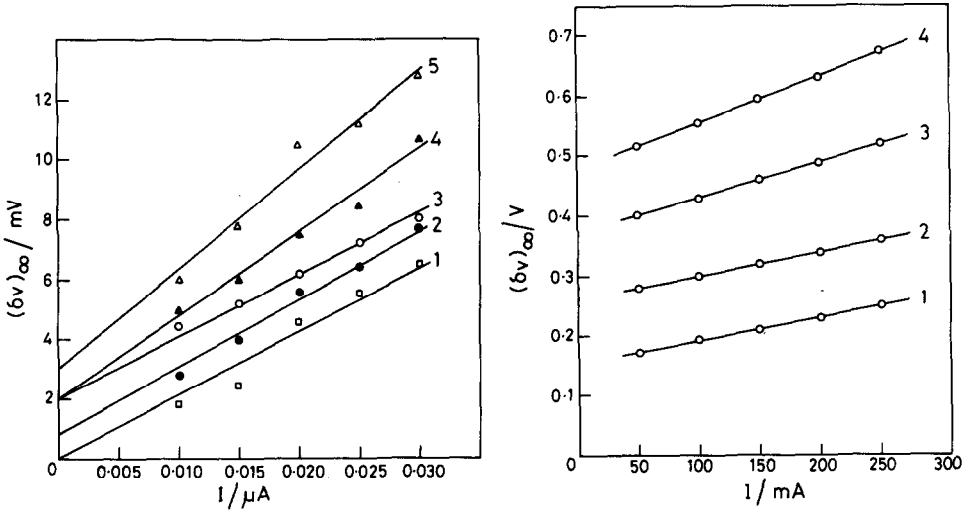

Fig. 8. Cell-voltage drop *vs.* discharge current in the range $4 \times 10^{-9}\ Q - 1.2 \times 10^{-9}\ Q$ for five Mg–MnO_2 dry cells. Each line obtained from a fresh cell. For clarity, curve 2 has been shifted vertically by +1 mV, curves 3, 4 by +2 mV, and curve 5 by +3 mV.

Fig. 9. Plot of cell-voltage drop *vs.* the discharge current in the range $2 \times 10^{-2}\ Q - 10^{-1}\ Q$ for four Mg–MnO_2 dry cells. Each line obtained from a fresh cell. For clarity, curves 1, 2, 3 and 4 have been shifted vertically by +0.1 V, +0.2 V, +0.3 V and +0.4 V, respectively.

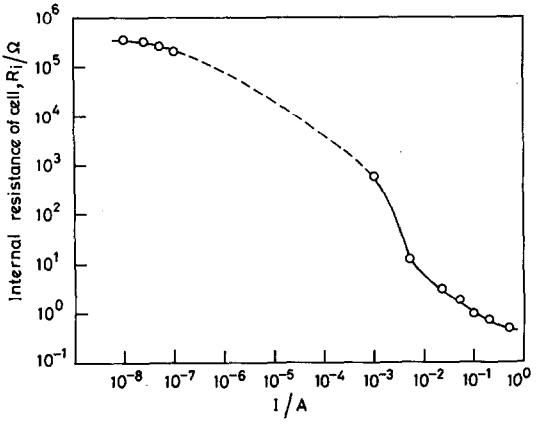

Fig. 10. Typical plot of internal resistance of Mg–MnO_2 dry cells *vs.* discharge current. Internal resistance was obtained from slope of lines presented in Figs. 8 and 9. The dashed line does not have experimental points.

It can be seen that there is a dramatic fall in the internal resistance by several orders of magnitude when the discharge current is of the order of 10^{-3} Q ampere or more. On the other hand, the value of R_i at discharge currents $\sim 10^{-8}$ Q ampere is a constant and high value. These facts clearly demonstrate the non-destructive character of the method proposed for the determination of the internal resistance of the protective film on the metal anode.

Film capacitance

Typical plots of $\ln\{d(\delta V)/dt\}$ *vs.* t and of $\ln\{(\delta V')\}$ *vs.* t derived from the transient data of Fig. 5 at different discharge currents for the same cell are shown in Figs. 11 and 12. Straight line plots are obtained, thus confirming the correctness of the theory.

From the slope of the straight lines in Figs. 11 and 12, and the data obtained on internal resistance, the value of C_1 can be evaluated by the method proposed above. The results for two cells are shown in Fig. 13.

The reasonable constancy of the value of C_1 over a wide range of test currents, and the effective value of C_1 per unit area of the anode, *viz.*, 2 - 3 μF cm^{-2}, point to the fact that what is thus obtained is, indeed, the interfacial capacitance of the film-covered anode/electrolyte or, simply, the film capacitance.

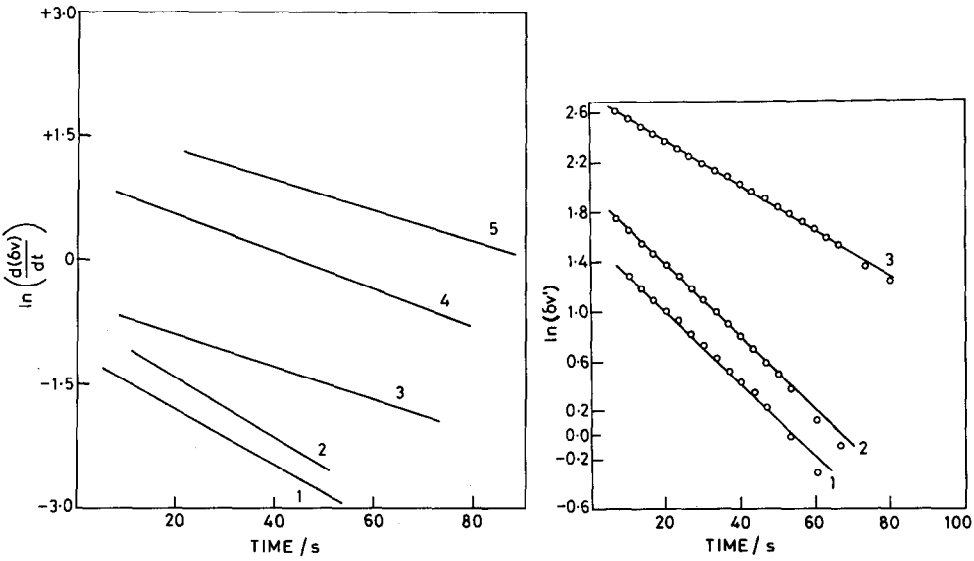

Fig. 11. Plot of $\ln(d(\delta V)/dt)$ *vs.* t at 1, 0.010; 2, 0.015; 3, 0.020; 4, 0.025; 5, 0.030 μA. Data were obtained from curves of the type shown in Fig. 5.

Fig. 12. Plot of $\ln \delta V'$ *vs.* t for the same cells as in Fig. 11 after terminating the transient discharge at 1, 0.010; 2, 0.015; 3, 0.025 μA.

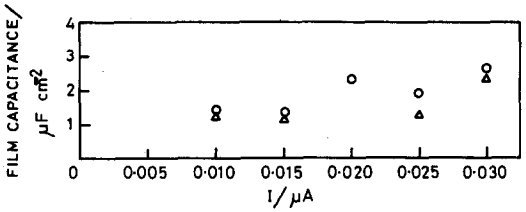

Fig. 13. Plot of film capacitance, C_1, *vs.* discharge current, I. ○, data calculated from the discharge transient; △, data from the open-circuit transient.

Conclusions

The results of the experiments clearly demonstrate that the film-resistance and double-layer capacitance at the anode of Mg–MnO_2 cells can be determined by the d.c. micropolarisation technique described in this paper. This method appears to be free from the uncertainties associated with pulse techniques, is non-destructive in character, and involves simple instrumentation easily adaptable for production-line testing of such cells. The method, although illustrated using Mg–MnO_2 cells, is, in principle, capable of being extended to other battery systems consisting of anodes covered by a resistive-film before discharge.

Since the film-resistance and film-capacitance are obtained by the method proposed for assembled battery-cells in a non-destructive way, possible failure modes relating to low-temperature passivation, cell dry-out on ageing, the development or presence of internal electronic shorts (soft shorts), etc., may also be identified.

List of symbols

α, β	Cathodic and anodic energy-transfer coefficient, respectively
η	Observed overpotential
E	Observed electrode potential
E_{rev}	Reversible electrode potential
E_a	Observed anode potential
$E_{a,cor}$	Anode potential under open-circuit conditions
E_c	Observed cathode potential
I	Current through anode/cell
I_o	Exchange current for redox process
I_{cor}	Corrosion current for corrosion reaction
I_{far}	Faradaic component of total current
I_{ch}	Non-faradaic/charging component of total current
V	Closed-circuit cell voltage
V_o	Open-circuit cell voltage
V_s	Closed circuit cell voltage under steady state conditions

V' Cell voltage during open circuit recovery
R_f Film resistance
R_i Total internal resistance of the cell
R_d Resistance of solution, separator and cathode mix
R_t Charge-transfer resistance
C_i Film capacitance
Q Numerical value of nominal ampere-hour capacity of the cell
δV $= V_o - V$, $\delta V' = V_o - V'$, $(\delta V)_\infty = (V_o - V)$ as $t \to \infty$

References

1 B. V. Ratnakumar and S. Sathyanarayana, *J. Power Sources, 10* (1983) 219.
2 S. Sathyanarayana and B. V. Ratnakumar, *J. Power Sources, 10* (1983) 243.
3 R. V. Moshtev, Y. Geronov and B. Puresheva, *J. Electrochem. Soc., 128* (1981) 1851.
4 R. V. Moshtev and Y. Geronov, *J. Power Sources, 8* (1982) 395.